



Georg R. Pesch, Fei Du, Michael Baune, Jorg Thöming

Influence of geometry and material of insulating posts on particle trapping using positive dielectrophoresis

Journal Article as: peer-reviewed accepted version (Postprint)

DOI of this document* (secondary publication): <https://doi.org/10.26092/elib/2471>

Publication date of this document: 21/09/2023

* for better findability or for reliable citation

Recommended Citation (primary publication/Version of Record) incl. DOI:

Georg R. Pesch, Fei Du, Michael Baune, Jorg Thöming,
Influence of geometry and material of insulating posts on particle trapping using positive dielectrophoresis,
Journal of Chromatography A, Volume 1483, 2017, Pages 127-137, ISSN 0021-9673,
<https://doi.org/10.1016/j.chroma.2016.12.074>

Please note that the version of this document may differ from the final published version (Version of Record/primary publication) in terms of copy-editing, pagination, publication date and DOI. Please cite the version that you actually used. Before citing, you are also advised to check the publisher's website for any subsequent corrections or retractions (see also <https://retractionwatch.com/>).

This document is made available under a Creative Commons licence.

The license information is available online: <https://creativecommons.org/licenses/by-nc-nd/4.0/>

Take down policy

If you believe that this document or any material on this site infringes copyright, please contact publizieren@suub.uni-bremen.de with full details and we will remove access to the material.

Influence of geometry and material of insulating posts on particle trapping using positive dielectrophoresis

Georg R. Pesch*, Fei Du, Michael Baune, Jorg Thöming¹

Chemical Engineering: Recovery and Recycling, University of Bremen and Center for Environmental Research and Sustainable Technology (UFT), Leobener Straße, 28359 Bremen, Germany

ARTICLE INFO

Article history:

Received 29 August 2016
Received in revised form
20 December 2016
Accepted 23 December 2016
Available online 26 December 2016

Keywords:

Insulator-based dielectrophoresis
Electrodeless dielectrophoresis
Microparticle manipulation
Particle trajectories
Polarization
Post array design rules

ABSTRACT

Insulator-based dielectrophoresis (iDEP) is a powerful particle analysis technique based on electric field scattering at material boundaries which can be used, for example, for particle filtration or to achieve chromatographic separation. Typical devices consist of microchannels containing an array of posts but large scale application was also successfully tested. Distribution and magnitude of the generated field gradients and thus the possibility to trap particles depends apart from the applied field strength on the material combination between post and surrounding medium and on the boundary shape.

In this study we simulate trajectories of single particles under the influence of positive DEP that are flowing past one single post due to an external fluid flow. We analyze the influence of key parameters (excitatory field strength, fluid flow velocity, particle size, distance from the post, post size, and cross-sectional geometry) on two benchmark criteria, i.e., a critical initial distance from the post so that trapping still occurs (at fixed particle size) and a critical minimum particle size necessary for trapping (at fixed initial distance). Our approach is fundamental and not based on finding an optimal geometry of insulating structures but rather aims to understand the underlying phenomena of particle trapping.

A sensitivity analysis reveals that electric field strength and particle size have the same impact, as have fluid flow velocity and post dimension. Compared to these parameters the geometry of the post's cross-section (i.e. rhomboidal or elliptical with varying width-to-height or aspect ratio) has a rather small influence but can be used to optimize the trapping efficiency at a specific distance. We hence found an ideal aspect ratio for trapping for each base geometry and initial distance to the tip which is independent of the other parameters.

As a result we present design criteria which we believe to be a valuable addition to the existing literature.

© 2016 Elsevier B.V. All rights reserved.

1. Introduction

Dielectrophoresis [1–3] is a promising particle manipulation technique. Up to now, it is mostly used in the biomedical industry, e.g., for characterization and manipulation of DNA [4], proteins [5], stem cells [6], and other bioparticles [7]. It has also been used in the assembly of nanotubes [8] and colloidal structures [9] and is investigated as a measure against colloidal membrane fouling in filtration processes [10–13]. It is label-free, does not require a net

charge on the particles, and can be applied using either ac or dc electric fields.

It is based on the interaction of an induced multipole (dipole, quadrupole, etc.) with an inhomogeneous electric field [14]: a particle subjected to an electric field will polarize, resulting in charge separation at the surface of the particle. If the excitatory field is inhomogeneous (i.e., unequal in magnitude on both sides of the particle), the Coulomb force which acts on each side of the particle is unequal. This results in a net force and thus movement of the particle towards regions of higher or lower electric field. The force direction depends on the relative polarizability of the particle in the surrounding medium, as expressed by the polarization coefficients [15], for example the well-known Clausius–Mossotti factor (first order polarization coefficient) for a perfectly spherical particle. If it is positive (negative), the particle is more (less) polarizable than the surrounding medium and the resulting force points

* Corresponding author.

E-mail addresses: gpesch@uni-bremen.de (G.R. Pesch), thoeming@uni-bremen.de (J. Thöming).

¹ Principal investigator.

towards higher (lower) electric field regions, thus towards (against) the electric field gradient, which is termed positive (negative) DEP.

The force magnitude acting on a spherical particle is directly proportional to the particle's volume and the gradient of the square of the electric field. Hence, movement of small particles requires large electric fields and rapid spatial electric field changes. A very prominent method for achieving such electric field gradients is insulator-based or electrodeless dielectrophoresis (as opposed to electrode dielectrophoresis) which is exploiting the fact that electric fields distort at material boundaries. When a stationary material boundary (usually termed obstacle or post) is introduced in an originally homogeneous electric field, polarization charges will accumulate at the boundary [16]. These charges themselves will generate an inhomogeneous electric field which is very suited to induce dielectrophoretic particle motion. Extension and magnitude of the generated field gradient depend on the difference in dielectric properties between the two materials and the shape of the boundary.

Among other arrangements (e.g., microchannel constrictions [17], single obstacles [18], or oil droplets as obstacles [19]) an array of insulating posts [20–22] is mostly used for field distortion in electrodeless DEP. Here, two cases can be considered: the majority of publications deals with the immobilization of particles exhibiting negative dielectrophoresis. In this case particles are usually immobilized in the gaps between posts due to an equality of dielectrophoretic and electrokinetic forces. These setups do not require pumps as the transversal movement through the separator is achieved using the effective electrokinetic force (EK, resulting from electroosmosis and electrophoresis). The negative DEP force points against the EK force and when both forces are equal in magnitude the particle becomes immobilized. Since the EK force depends on the direction of the excitatory field, these setups usually use dc potentials [23] or dc-biased ac potentials [22]. They are mostly used to achieve chromatographic separation of particle mixtures by size or dielectric properties for sample preparation or analysis [22–25].

A smaller part of the publications uses positive dielectrophoresis (cf. Fig. 1a) to trap particles at points of maximum electric field strength at the surface of the posts [26–29]. They either use EK (and thus dc or dc-biased ac voltage [26]) or rely on pumps [27,28] for particle transport through the setup. In a certain range it is possible to adjust the dielectrophoretic answer of a particle (whether positive or negative) by varying the frequency of the applied ac field or by varying the suspension's conductivity [30]. Nevertheless, most biological particles exhibit negative DEP in their respective (conductive) buffer solution over a wide frequency range whereas technical particles (such as metal particles or most submicron latex spheres at frequencies in the kHz range and below [30]) mostly exhibit positive DEP in pure water.

In the past, positive iDEP or electrodeless systems have been used for the immobilization of DNA as well as some proteins. For example, Prinz et al. [31] trapped *Escherichia coli* chromosomes after lysing in micro constrictions. Chou et al. [32] trapped single- and double-stranded DNA using electrodeless DEP traps. They also presented a model for the polarization behavior of DNA, which cannot be described by the Clausius–Mossotti factor. This has been advanced by Regtmeier et al. [33,34] also using electrodeless DEP traps. Nakano et al. [35] trapped immunoglobulin G and bovine serum albumin using positive DEP in arrays of insulating posts. Recently, Mata-Gómez et al. [36] separated PEGylated RNase A from unreacted RNase in arrays of rhomboidal posts exploiting the dependence of the positive DEP force of PEGylated and the unreacted RNase species on the size of the molecule.

Kazemlou and Nazemifard [29] described the influence of positive DEP on the electrophoretic separation of DNA in micro-fabricated post arrays, a phenomenon which has been ignored by

most studies but can be used to account for some inexplicable band broadening. Here, the pDEP effects are undesired and should be minimized, quite contrary to the aim of most iDEP studies. Hence, it is necessary to elucidate the mechanisms of positive particle trapping in arrays of insulating posts and other electrodeless DEP devices.

Insulator-based or electrodeless DEP emerged to be a prominent method to achieve particle and cell separation and characterization; a somewhat more detailed literature study on this topic could be found in the excellent reviews by Regtmeier et al. [37] and Srivastava et al. [38].

We have recently published an electrically switchable filtration process based on the concept of insulator-based dielectrophoresis [39]. In this, we used polyethylene filters as electric field obstacles: the porous material is sandwiched between two electrodes and becomes polarized due to the excitatory field. The resultant field gradients were used to DEP trap and thus separate particles that experience positive DEP from a solution which is pumped through the filter. Other studies [40–42] used glass beads as porous medium in between electrodes for DEP trapping. We, however, were the first to publish a DEP filter using the inverse structure, a foam or sponge. Albeit receiving very promising results, the study itself was not based on deep insight on the polarization behavior of the porous medium. Instead of consciously designing the porous medium we used commercially available polymer filters for conducting a proof-of-principle study. Recent studies [16,21,24] indicate that the distribution and the intensity of the generated electric field gradient strongly depend on the shape of the boundary and the two involved materials (i.e., the material of the liquid medium and the material of the obstacle or post).

The design of a porous medium optimized towards dielectrophoretic particle separation requires understanding of its polarization behavior and how this alters the excitatory electric field. LaLonde et al. [24] and subsequently Saucedo-Espinosa and Lapizco-Encinas [21] presented very thorough application-oriented studies with iDEP channels using insulating posts to find ideal post geometries and spacings.

LaLonde et al. [24] compared the minimum required voltage for iDEP trapping in channels using posts with diamond-shaped and circular cross sections with different cross-sectional width-to-height ratios. They found that diamonds outperform circles in every case and that such diamonds (short diamonds) whose dimension parallel to the flow direction (width) is shorter than the dimension perpendicular to the flow (height) require the least voltage for iDEP trapping of particles. Saucedo-Espinosa and Lapizco-Encinas [21] presented a method to find a flow channel with an optimized arrangement of insulating posts. For each cross-sectional base geometry (diamond, circle and square) they optimized the geometry of the setting using COMSOL simulations. Subsequently they experimentally compared the three optimized setups and found that the optimized square posts require the least voltage for iDEP trapping, followed by the optimized circles, and concluded by the optimized diamonds.

In a previous study [16] we presented a method to mathematically describe electrically polarized posts using an infinite series of multipoles. We used this multipole expansion to describe the influence of the cross-sectional geometry (rhomboidal, cf. Fig. 1b and elliptical, cf. Fig. 1c), the cross-sectional width-to-height ratio (aspect ratio, AR) and the ratio between the permittivity of the surrounding medium and the permittivity of the post material (permittivity ratio, Fig. 1d and e) on the polarization behavior of the post. The polarization behavior describes the resulting DEP force on arbitrary particles in the vicinity of the post. Depending on how the post polarizes, the resulting forces are either long range but do not show a large maximum close to the post or short-range with a comparably large maximum at the post's surface (we found quite

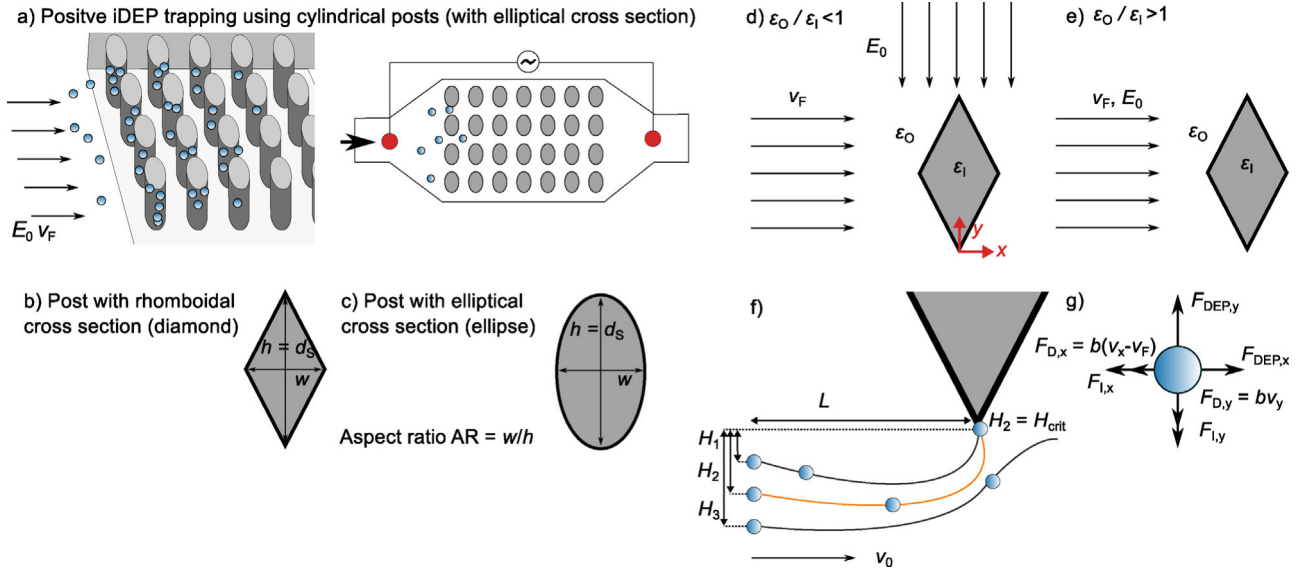


Fig. 1. Schematic overview of the evaluation method. (a) A 3d sketch of an insulator-based DEP channel and trapping of particles in such channels due to positive DEP. Also shown is, as an example, a top view of such a channel with cylindrical electrodes; particles are not to scale. (b) and (c) The two base geometries (rhomboidal or diamond, b and elliptical, c) investigated in this study. The aspect ratio $AR = w/h$ is the width-to-height ratio of the cross-section. The characteristic dimension d_s of the post is the larger of either w or h , in the case of this manuscript ($AR < 1$) it is always $d_s = h$. (d) and (e) Ideal constellations of field, flow, and AR depending on the ratio of the post's permittivity ϵ_1 and the surrounding medium's permittivity ϵ_0 ; explanation in text. (f) A qualitative sketch of three particle trajectories with three different starting distances to the tip in y -direction, H_1 , H_2 , and H_3 . Also shown is the critical distance-to-tip $H_{crit} = H_2$ at which trapping just occurs. (g) The force balance acting on the particle due to the fluid drag ($F_{D,(x,y)}$), dielectrophoresis ($F_{DEP,(x,y)}$), and inertia ($F_{I,(x,y)}$).

similar correlations for the force due to interdigital electrode arrays [43]). The present manuscript continues this work by evaluating the particle trapping behavior of such posts. We use a single-obstacle approach to assess the influence of the post's geometry and material on the particle trapping behavior. We focus on the positive DEP particle trapping in which fluid flow is achieved using pumps (model system of our original filtration process).

Instead of investigating the entire array of posts we focus on single posts and single particles in order to understand how capable the undisturbed short- and long-range interactions of a single post are for manipulating particle trajectories.

To do so we simulate trajectories of particles which are flowing past the post and investigate how the particles are influenced by the DEP force generated by the post. We place the post in a steady fluid flow containing particles so that the particles are flowing past the post. Due to positive DEP the particles will be attracted and depending on key parameters (fluid flow velocity, particle size, and excitatory field strength) the particles will either be trapped by the post (due to DEP) or flow past the post (due to the drag force exerted by the fluid). By varying the key parameters and investigating whether particles are trapped or not (depending on the geometrical properties of the post) we elucidate the trapping potential of posts depending on their geometrical properties.

Towards the end of the manuscript we additionally present a comparison of our key results with results obtained using two opposing posts.

2. Theoretical background

2.1. Dielectrophoresis

To describe the force \mathbf{F}_{DEP} acting on a spherical particle with radius a in an inhomogeneous electric field, the simple point-dipole approximation gives, in the most cases, reasonably accurate results [14]:

$$\langle \mathbf{F}_{DEP} \rangle = 2\pi\epsilon_0\epsilon_m a^3 \text{Re}[f_{CM}] \nabla |\mathbf{E}_{RMS}|^2. \quad (1)$$

Here, $\langle \rangle$ denotes the time averaged value, ϵ_0 the absolute permittivity of free space, ϵ_m the relative permittivity of the medium the particle is in, $\text{Re}[f_{CM}]$ the real part of the Clausius–Mossotti factor, and \mathbf{E}_{RMS} the vector of the electric field RMS (root mean square) value. The equation is derived on the assumption of a spherical particle whose radius is small compared to the spatial change of the field. In all other cases higher-order polarization terms or the Maxwell-Stress-Tensor have to be used [44]. The Clausius–Mossotti factor is a function of the complex permittivities of the particle (subscript P) and the medium (subscript M) and the real part $\text{Re}[f_{CM}]$ describes the particle's effective polarizability:

$$f_{CM} = \frac{\tilde{\epsilon}_P - \tilde{\epsilon}_M}{\tilde{\epsilon}_P + 2\tilde{\epsilon}_M}, \quad (2)$$

$$\tilde{\epsilon} = \epsilon_0\epsilon_r + \frac{\sigma}{j\omega}. \quad (3)$$

The real relative permittivity is ϵ_r and σ the conductivity. The imaginary number is denoted by j , whereas $\omega = 2\pi f$ is the angular frequency. The real part of the Clausius–Mossotti factor $\text{Re}[f_{CM}]$ is bound between -0.5 and 1 and gives the direction and magnitude of the force.

2.2. Electric fields and post polarization

As the electric field has a zero curl, the field vector \mathbf{E} can be expressed as the negative gradient of the scalar *electric potential* [45]:

$$\mathbf{E} = -\nabla\Phi. \quad (4)$$

In case of charge-free space Φ has to fulfill Laplace equation:

$$\Delta\Phi = 0. \quad (5)$$

In the case of harmonically oscillating excitation, Eq. (5) is only valid if the complex permittivity $\tilde{\epsilon}$ (which is the actual material constant for the distribution of harmonically oscillating electric fields through materials) is constant in the considered domain. For the special case of a single post in a homogeneous electric field

applied perpendicular to the longitudinal axis of the post it is convenient to define the electric potential in 2d polar coordinates, $\Phi(r, \varphi)$ [16]. This is justified since changes of the field along the channel depth are negligible [46]. Since the superposition principle applies, the electrostatic potential can be expressed as the sum of the polarization potential Φ_{pol} and the potential due to the applied homogeneous field Φ_0 :

$$\Phi = \Phi_{\text{pol}} + \Phi_0. \quad (6)$$

The polarization potential for posts with symmetrical cross section can be expressed as the infinite sum of polarization coefficients [16]:

$$\Phi_{\text{pol}} = \sum_{n=1}^{\infty} \frac{p_n \sin(n\varphi)}{r^n}, \quad (7)$$

where p_1 stands for the dipole polarization, p_2 for the quadrupole polarization, p_3 for the octupole polarization, and so on. Depending on the ratio of permittivities between the post and the surrounding medium, on the cross-sectional geometry, and on the strength and direction of the excitatory field, the distribution and magnitude of the polarization coefficients differs. A list of dimensionless coefficients as a function of permittivity ratio and geometry can be found in our previous publication [16].

By differentiating Eqs. (6) and (7) twice we can find an analytical expression for the term $\nabla|\mathbf{E}|^2$ of Eq. (1) due to a single polarized post in a homogeneous electric field [16]:

$$\nabla|\mathbf{E}|^2 = (\partial_x|\mathbf{E}|^2, \partial_y|\mathbf{E}|^2)^T, \quad (8a)$$

$$\begin{aligned} \partial_x|\mathbf{E}|^2 = & - \sum_{n=1}^{\infty} \sum_{k=1}^{\infty} \frac{kn(n+1)}{2r^{k+n+3}} p_n p_k \cos((k-n-1)\varphi) \\ & - \sum_{n=1}^{\infty} \frac{n(n+1)}{2r^{n+2}} E_0 p_n \cos((n+2)\varphi), \end{aligned} \quad (8b)$$

$$\begin{aligned} \partial_y|\mathbf{E}|^2 = & \sum_{n=1}^{\infty} \sum_{k=1}^{\infty} \frac{kn(n+1)}{2r^{k+n+3}} p_n p_k \sin((k-n-1)\varphi) \\ & - \sum_{n=1}^{\infty} \frac{n(n+1)}{2r^{n+2}} E_0 p_n \sin((n+2)\varphi). \end{aligned} \quad (8c)$$

Here, ∂_n is short for $\partial/\partial n$ and a superscript T denotes a vector's transpose. Two polarization coefficients are present in Eq. (8), p_n and p_k , because \mathbf{E} is squared and it is thus necessary to go through a double sum. This allows us to calculate the force on a spherical particle in the vicinity of a polarized post if we assume that the dipole approximation delivers reasonably accurate results.

3. Materials and methods

To evaluate and compare the posts trapping potential, we developed a method which is based on simulating a critical particle diameter $d_{p,\text{crit}}$ and/or a critical distance from the post's tip H_{crit} . This allows for a quantitative comparison of all evaluated geometries. For the study we compare two post base types: one with rhomboidal (Fig. 1b) and one with elliptical (Fig. 1c) cross section. The aspect ratio (AR), i.e., the cross-sectional width-to-height ratio ($\text{AR} = w/h$), is varied between 0.1 and 1, while the height is kept constant at 1. For real dielectrics (with finite conductivity), the critical material property for the distribution of electric fields is the complex permittivity $\tilde{\epsilon}$. For simplicity we ignore the complex part of the permittivity of the medium and the post (and

hence assume ideal non-conductive dielectrics, which would be a reasonable approximation for isolators; nevertheless, we assume ideal non-conductors, without loss of generality, for simplifying the calculation process).

For the analysis we use the ratio between the medium's (outside, O) permittivity ϵ_O and the post's (inside, I) permittivity, ϵ_I , ϵ_O/ϵ_I , as material property parameter. In this study it is varied between 10^{-4} and 1. If ϵ_O/ϵ_I is smaller than one, the points of maximum electric field appear at the two points parallel to the applied field. If, in contrast, $\epsilon_O/\epsilon_I > 1$, the points of maximum electric field will appear at the two points perpendicular to the applied field. It is therefore convenient to vary the direction of the excitatory field depending on ϵ_O/ϵ_I so that the points of maximum field are always perpendicular to the flow direction (cf. Fig. 1d and e). Since all results will be identical for posts that have both, the inverse ϵ_O/ϵ_I and the inverse aspect ratio, we only consider such posts with $\text{AR} < 1$ and $\epsilon_O/\epsilon_I < 1$ as discussed in our previous publication [16]. The posts are placed in a homogeneous electric field and fluid flow. We assume (and calculated) creeping flow (the Reynolds number $Re = (\rho \cdot v_F \cdot d_S)/\eta_F$ is much smaller than 1 in all cases considered) so that the fluid flows perpendicular to the tip of the post with a velocity of v_F . We initialize (technically speaking) particles of size d_p in the flow at distance L in x -direction and distance H in y -direction of the tip (cf. Fig. 1f). The fluid will drive the particles in x -direction past the tip of the post while they will be simultaneously attracted due to a DEP force towards the tip. The entire force balance on the particle with diameter $d_p = 2a$ and density ρ_p in a fluid with viscosity η_F in vector notation reads (cf. Fig. 1g):

$$\mathbf{F}_I = \mathbf{F}_D + \mathbf{F}_{\text{DEP}}, \quad (9a)$$

$$\frac{\partial^2 \mathbf{x}}{\partial t^2} = -\frac{18\eta_F}{\rho_p d_p^3} \left(\frac{\partial \mathbf{x}}{\partial t} - \mathbf{v}_F \right) + \frac{3\epsilon_0 \epsilon_m \text{Re}[f_{\text{CM}}]}{2\rho} \nabla |\mathbf{E}_{\text{RMS}}|^2 \quad (9b)$$

with $\mathbf{x} = (x, y)^T$ being the particle's position vector, $\mathbf{F}_I = m_p (\partial^2 \mathbf{x} / \partial t^2)$ being the inertia force with the particle's mass m_p , $\mathbf{F}_D = -3\pi\eta_F d_p \mathbf{v}_{\text{rel}}$ the Stokes drag force, $\mathbf{v}_{\text{rel}} = (\partial \mathbf{x} / \partial t - \mathbf{v}_F)$ the relative velocity between the particle ($\partial \mathbf{x} / \partial t$) and the fluid (\mathbf{v}_F) and $\mathbf{F}_{\text{DEP}} = \langle \mathbf{F}_{\text{DEP}} \rangle$ the time-averaged DEP force (Eq. (1)). This is an ODE of second order which can be solved in this specific case using the initial conditions:

$$\mathbf{x}_0 = (-L, -H)^T, \quad (10a)$$

$$\left(\frac{\partial \mathbf{x}}{\partial t} \right)_0 = (v_F, 0)^T, \quad (10b)$$

$$\left(\frac{\partial^2 \mathbf{x}}{\partial t^2} \right)_0 = (0, 0)^T. \quad (10c)$$

This assumes that the origin of the underlying coordinate system is placed at the bottom tip of the obstacle.

The polarization coefficients for this configuration have been calculated previously and they are only valid for a specific obstacle size and exciting field strength (they have been calculated dimensionless in Pesch et al. [16]). Hence, to acquire the coefficients for the desired unperturbed field strength E_0 it is necessary to multiply all coefficients by E_0 . Further, we assumed arbitrary length units in our previous publication so that all obstacles have a characteristic dimension d_S (Fig. 1b and c, the larger of either w or h , here $d_S = h$ as $\text{AR} < 1$) of 1. To evaluate a post which has, for example, a characteristic dimension of $500 \mu\text{m}$, 1 length unit equals $500 \mu\text{m}$. All other in the study involved parameters (such as E_0 or ϵ_0) have to be recalculated so that all units of length are expressed in this previously defined arbitrary length unit.

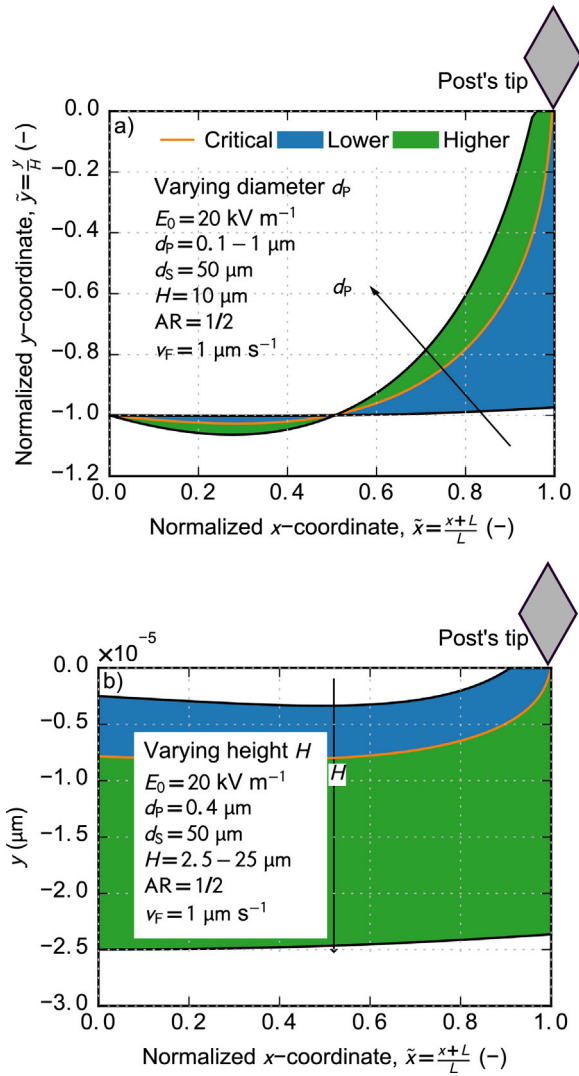


Fig. 2. Typical particle trajectories obtained by numerical calculations, i.e., solving Eqs. (9b) and (10), for a rhomboidal post and particles having a Clausius-Mossotti factor of 1 at an applied field of $E_0 = 20 \text{ kV m}^{-1}$. The posts lower tip is located at $(1.0, 0.0)$ as indicated. (a) The normalized y -coordinate, $\tilde{y} = y/H$, as a function of the normalized x -coordinate, $\tilde{x} = (x+L)/L$ for different particle diameters d_p at constant H . (b) The absolute y -coordinate as a function of \tilde{x} for different starting distances from the tip H at constant particle diameter d_p . The green and blue shaded areas show where trajectories with d_p and H higher and lower, resp., than the critical value $d_{p,crit}$ and H_{crit} lie. The two black lines give the trajectories for the smallest and largest parameter (d_p in (a) and H in (b)) calculated. (For interpretation of the references to color in this figure legend, the reader is referred to the web version of the article.)

We solved Eq. (9b) with the initial conditions (10) using the LSODAR wrapper from odespy Python package.² Integration stops as soon as the x - or y -coordinate hit 0.

In order to obtain criteria for assessing trapping performance critical parameters were extracted from particle trajectory calculations. In Fig. 2 typical particle trajectories (as calculated from Eq. (9b)) for different values of d_p at constant H of $10 \text{ }\mu\text{m}$ (Fig. 2a) and different values of H at constant d_p of 400 nm (Fig. 2b) are shown. Other values are an excitatory field strength E_0 of 20 kV m^{-1} , a post dimension of $50 \text{ }\mu\text{m}$ and an aspect ratio of $1/2$. Fluid flow velocity $v_F = 1 \text{ }\mu\text{m s}^{-1}$. Here, and in all subsequent figures, we assume water as the suspending medium with $\eta_F = 1 \text{ mPa s}$ and polystyrene

particles with density $\rho_p = 1050 \text{ kg m}^{-3}$. In this figures, all particle trajectories that reach $\tilde{x} = (x+L)/L = 1$ without reaching $y = 0$ will pass the tip without being trapped (blue shaded area in Fig. 2a and green shaded area in Fig. 2b); contrary, all trajectories reaching $y = 0$ before $\tilde{x} = 1$ are trapped (green shaded area in Fig. 2a and blue shaded area in Fig. 2b). Due to the cubic dependence of F_{DEP} on d_p , at constant H (Fig. 2a) small particles will pass the post without trapping (blue shaded area) whereas particles that are bigger (green shaded area) than a critical particle diameter $d_{p,crit}$ (orange trajectory) become trapped. Similarly, at constant d_p , a critical initial distance-to-tip H_{crit} exists (Fig. 2b, orange trajectory and also schematically depicted in Fig. 1f). Particles that start closer to the tip than H_{crit} ($H < H_{crit}$ in Eq. (10a), blue shaded area) become trapped, whereas particles with $H > H_{crit}$ (green shaded area) will pass the post untrapped. The DEP force in y -direction, $F_{DEP,y}$ does not always point towards the tip. At small H (particles start close to the tip in y -direction), particles will first be repelled by the tip (Figs. 2a and top black line in 2b) before they reach an area at which they become attracted (e.g. $\tilde{x} > \sim 0.25$ in Fig. 2a).

Please note that we require applicability of the point-dipole model and particles to have a CM factor of 1 for the evaluation to be precise. We therefore have no direct constraint on the applied frequency, but this of course could influence particles' CM factor. Examples for particles having a CM factor of 1 are metal particles at frequencies below the RC frequency [47] or submicron latex particles in low conductivity solutions [30].

4. Results and discussion

The trajectories presented in Fig. 2 were used to extract the results presented in this section. Each critical starting distance to the tip or critical particle diameter, H_{crit} or $d_{p,crit}$, respectively, have been extracted from a series of particle trajectories which have been evaluated towards finding the critical trajectory.

4.1. Analytical validation

The validation of the numerical solution was performed by comparing simulated critical particle diameters with critical particle diameters obtained by applying the analysis method on the analytical solution for the post polarization (Fig. 3). In the figure, the critical particle diameter $d_{p,crit}$ as a function of the ratio between the medium's and the post's permittivity, ϵ_0/ϵ_1 , is plotted for different posts: two ellipse posts (blue circles) with an AR of 1 (void symbols) and 0.2 (filled symbols) and two diamond posts (orange diamonds) with AR of 1 (void symbols) and 0.2 (filled symbols). The solid black line shows the results of the analysis when the analytical solution for the first-order polarization coefficient of the AR 1 ellipse is put in [16]:

$$p_1 = \frac{1 - \epsilon_0/\epsilon_1}{1 + \epsilon_0/\epsilon_1} \quad (11)$$

The post diameter (or characteristic dimension) d_s is $50 \text{ }\mu\text{m}$, the volume flow $v_F = 4 \text{ }\mu\text{m s}^{-1}$, the initial y -distance to the tip $H = 3.75 \text{ }\mu\text{m}$ and the excitatory field strength $E_0 = 40 \text{ kV m}^{-1}$. The analytical solution and the solution due to the coefficients obtained by numerical integration agree very well. The best trapping behavior of all posts is found when the permittivity between the surrounding medium ϵ_0 and the permittivity of the post ϵ_1 differs by several orders of magnitude, as evident from the low $d_{p,crit}$ at high ϵ_0/ϵ_1 . A specific $d_{p,crit}$ minimum is reached at a certain ϵ_0/ϵ_1 , depending on the system properties; in this case, the minimum is reached between $\epsilon_0/\epsilon_1 = 1 \times 10^2$ and 1×10^3 . This is because the strength of the resulting multipole (due to the post polarization) increases with increasing difference of ϵ_0/ϵ_1 from unity. This increase is not infinite as there is a maximum amount

² <http://hplgit.github.io/odespy/doc/api/odepack.html>.

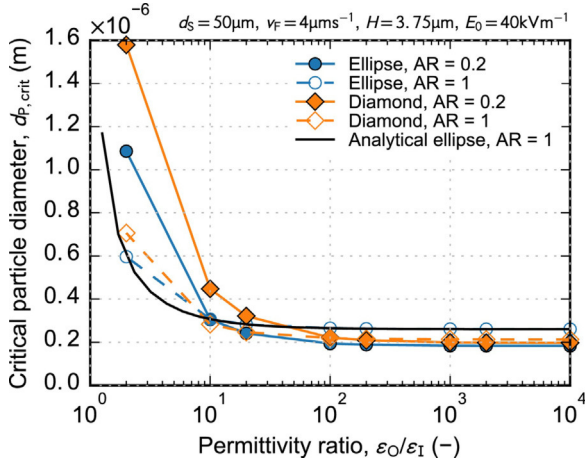


Fig. 3. Critical particle diameter $d_{p,crit}$ as a function of permittivity ratio ϵ_0/ϵ_1 for posts with elliptical (blue circles) and rhomboidal (orange diamonds) cross section with an aspect ratio AR of 0.2 (filled symbols) and an AR of 1 (void symbols). The solid black line shows the analytical solution, that is, the solution from the presented analysis framework when the analytical solution for the first-order polarization coefficient for an ellipse with AR of 1 is put in. (For interpretation of the references to color in this figure legend, the reader is referred to the web version of the article.)

of polarization as discussed by us [16] and $d_{p,crit}$ becomes constant with ϵ_0/ϵ_1 at $\epsilon_0/\epsilon_1 > 10^2$.

4.2. Distribution of polarization among multipole coefficients

The resulting overall polarization of the specific post will be distributed between multipoles with varying order (i.e., polarization coefficient p_n with $n = 1$ dipole, $n = 2$ quadrupole, $n = 3$ octupole, etc.); the physical representation of this multipoles was discussed by us [16] and for objects with spherical symmetry by Green and Jones [15]. The distribution of the overall polarization on each specific polarization term ($n = 1, 2, 3, \dots$) depends on the shape of the boundary of the cross section, whereas the overall magnitude of the polarization ($\sum_{n=1}^{\infty} p_n$) depends on the permittivity ratio. A post with circular cross section and AR = 1 has only a $n = 1$ (dipole) polarization; with increasing variation of the cross-sectional geometry from a perfect circle the higher-order polarization terms become more significant whereas the first-order polarization term loses significance.

The resulting force F_{DEP} (Eq. (1)) due to the inhomogeneous polarization field (Eq. (8)) is always strongest at the post surface and decays with increasing distance from the post. With increasing order n of the polarization term p_n , the maximum value at the post surface and the decay (slope) increase, i.e., with increasing n the force has a stronger maximum at the surface but is weaker at distance from the post because it decays faster with the distance from the post's surface.

This explains the sequence of $d_{p,crit}$ for the four investigated posts at the maximum ($\epsilon_0/\epsilon_1 > 1 \times 10^3$): the ellipse (AR=0.2) performs best, followed by the diamond (AR=0.2), followed by the diamond (AR=1), and the ellipse (AR=1) performs the worst of all four investigated posts. Depending on the initial distance to the tip H , this sequence changes because the distribution of the resulting multipole is different for all four investigated posts and thus also the maximum value and the decay with distance from the tip.

Each resulting multipole is defined by one polarization coefficient p_n . The development of each specific polarization coefficient with ϵ_0/ϵ_1 differs, i.e., the higher order n of coefficient p_n is, the faster it approaches 0 when ϵ_0/ϵ_1 goes towards unity (or, the steeper the slope). Hence, the more higher-order polarization coefficients are involved in the description of the overall

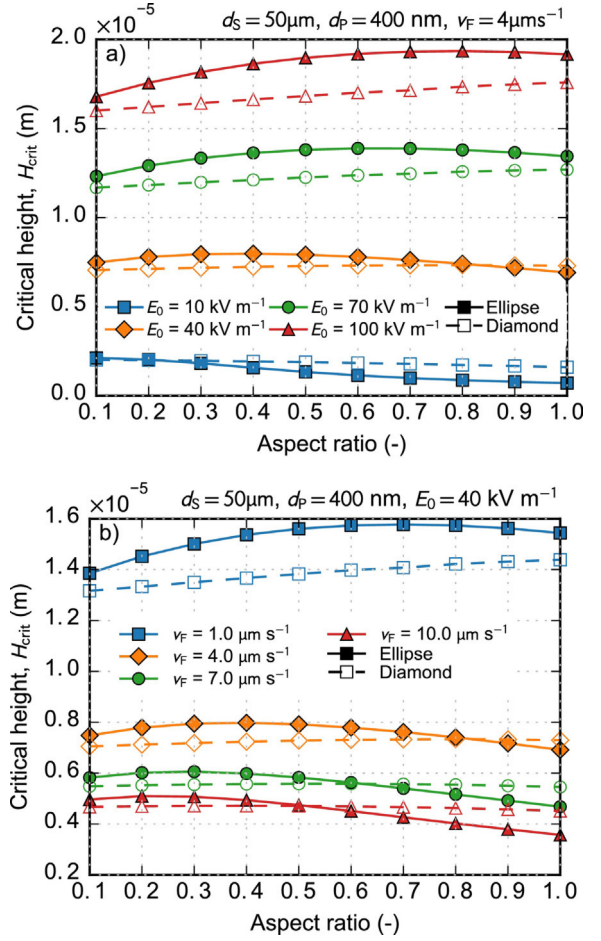


Fig. 4. Critical separation height H_{crit} as a function of aspect ratio for posts with elliptical (solid line with filled symbols) and rhomboidal (dashed line with void symbols) cross section for varying excitatory field strengths E_0 (a) and varying volume flow v_f (b). The post diameter d_s is the longer dimension of either w or h . As $AR = w/h < 1$, $d_s = h$ and independent of AR. It is also called characteristic dimension of the post.

polarization of the post, the faster the resulting $d_{p,crit}$ rises when ϵ_0/ϵ_1 goes to unity. Therefore, at $\epsilon_0/\epsilon_1 = 2 \times 10^0$ (very close to unity), the post with the least higher-order polarization terms (ellipse, AR=1) performs the best (lowest $d_{p,crit}$) and the post with the most higher-order polarization terms (diamond, AR=0.2, i.e., highest difference of the cross section from a perfect circle of all four investigated objects) performs the worst (highest $d_{p,crit}$).

4.3. Influence of key design and operational parameters

To investigate the influence of the key design parameters on the trapping potential of the posts, we extracted the critical starting distance from the tip H_{crit} as a function of the cross-sectional aspect ratio AR (Fig. 4) for different excitatory electric field strengths (Fig. 4a, $E_0 = 10\text{--}100 \text{ kV m}^{-1}$) and different fluid flow velocities (Fig. 4b, $v_f = 1\text{--}10 \text{ } \mu\text{m s}^{-1}$). Here, solid symbols together with the solid lines denote elliptical posts whereas void symbols with dashed lines denote rhomboidal posts.

With increasing excitatory field strength E_0 (Fig. 4a), H_{crit} increases as well. This is because a higher E_0 results in a stronger polarization of the post (as described in Section 3, the p_n are multiplied by E_0). Hence, particles can start further away from the post tip and still become attracted (overall force on the particle is stronger). Generally, the elliptical posts perform better (higher H_{crit}) and they appear to have an optimal aspect ratio (maximum in H_{crit}). Contrary to all other parameter values, the rhomboidal post

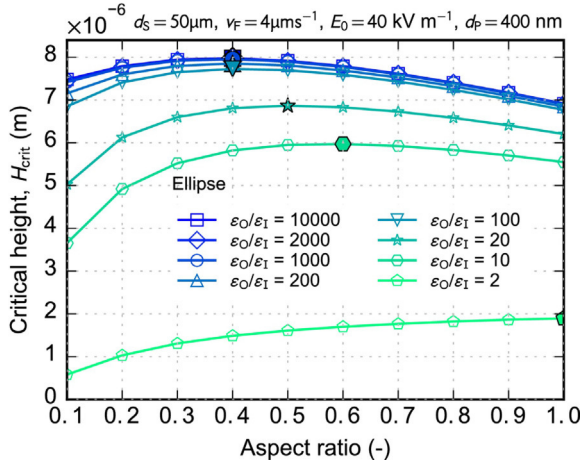


Fig. 5. Critical separation height H_{crit} as a function of the aspect ratio AR for elliptical posts and 8 different permittivity ratios ϵ_0/ϵ_1 from $2 \cdot 10^4$. The maxima are indicated by filled symbols.

performs better than the elliptical at the lowest E_0 . Here, H_{crit} is the overall lowest (thus particles start closest to the tip). In this case, the rhomboidal posts perform better, because they have stronger higher-order polarization terms than elliptical posts. Their resulting force field is thus stronger close the post but decays faster with distance than for an elliptical post. Hence, they perform better at closer distances (lower H_{crit}).

The curves look similar when E_0 is fixed at 40 kV m^{-1} and the particle diameter d_p is varied between 100 nm and 1000 nm (shown in Supplementary material, section 1). This indicates that the solution for this specific case is independent of inertia (due to the small particle mass); eliminating $\partial^2 \mathbf{x}/\partial t^2$ from Eq. (9b) (we assume it is constant) and solving for $\partial \mathbf{x}/\partial t$ (the steady state velocity) yields one single term that is $\partial \mathbf{x}/\partial t \propto d_p^2 \nabla |\mathbf{E}|^2$. Hence, if all other parameters are constant one could, for example, trap particles half the size by doubling the applied voltage.

The variation of the fluid velocity v_f (Fig. 4b) yields quite similar results with a reversed sequence. Then, with increasing v_f the H_{crit} decreases as particles will move faster past the post in x -direction and thus have less time to move towards the tip in y -direction. Again, for configurations with large H_{crit} , the elliptical post performs generally better (larger H_{crit}) than the rhomboidal post. This changes with decreasing H_{crit} ($v_f = 4\text{--}10 \text{ }\mu\text{m s}^{-1}$). Then, a transition with AR is found: For low AR, the ellipse performs better whereas for higher AR, the diamonds perform better. The cross over moves towards smaller AR with decreasing H_{crit} (increasing v_f). It is assumed that at even smaller H_{crit} the diamonds will always outperform the elliptical posts.

In addition, the dependence of the critical initial distance to the tip (H_{crit}) on the characteristic dimension is given in Supplementary material, Fig. S1. From the figures combined it appears that all outer parameters (E_0 , d_p , v_f , and d_s) have a quite similar impact on the H_{crit} (with a tendency that d_s having the most impact, followed by v_f and E_0 and d_p having the least impact) when varied by one order of magnitude, whereas the aspect ratio AR has a much smaller impact when varied between 0.1 and 1.

4.4. Influence of permittivity ratio

Furthermore, we investigated how H_{crit} varies with the permittivity ratio ϵ_0/ϵ_1 (Fig. 5) for a post with elliptical cross section. With increasing deviation of the ϵ_0/ϵ_1 from unity the H_{crit} generally increases for all AR from values around $0.5\text{--}2 \text{ }\mu\text{m}$ at $\epsilon_0/\epsilon_1 = 2.0$ to $7\text{--}8 \text{ }\mu\text{m}$ at $\epsilon_0/\epsilon_1 = 10^4$ (increasing trapping performance). This

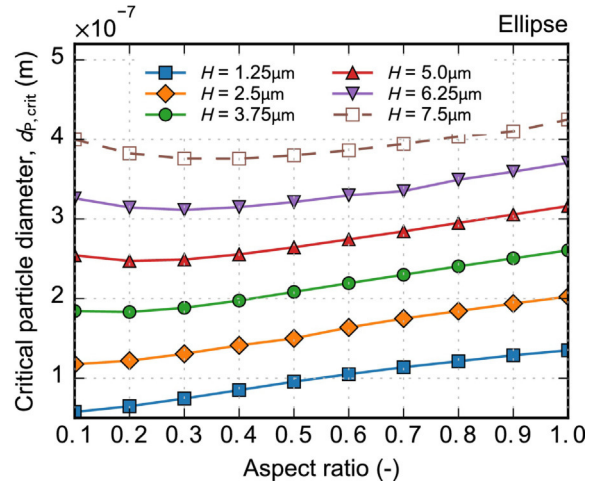


Fig. 6. Critical particle diameter $d_{p,\text{crit}}$ as a function of aspect ratio for an elliptical post and different starting distances in y -direction H from $1.25 \text{ }\mu\text{m}$ to $7 \text{ }\mu\text{m}$. Other parameters are $d_s = 50 \text{ }\mu\text{m}$, $v_f = 4 \text{ }\mu\text{m s}^{-1}$, $E_0 = 40 \text{ kV m}^{-1}$, and $d_p = 400 \text{ nm}$.

is analogous to Fig. 3. One can imagine that all curves end at 0 for AR being (hypothetically, but not possible) 0. Then, all curves have a H_{crit} -maximum (and thus optimal aspect ratio) which moves towards larger AR with ϵ_0/ϵ_1 coming closer towards unity. The reason for this maximum is rooted in the fact that with increasing amount of higher-order polarization terms (that means, comparably large p_n values for large n) a post performs better in trapping particles very close to the post but performs worse if particles are at distance from the post. The more AR deviates from 1, the more higher-order polarization terms a structure has. As already discussed in Fig. 3, with increasing n of the p_n (thus, with increasing order of the polarization coefficient) its slope with ϵ_0/ϵ_1 increases. This means, it will fall more than linear with $|\log_{10} \epsilon_0/\epsilon_1|$ when ϵ_0/ϵ_1 is close to unity. Thus, when ϵ_0/ϵ_1 comes closer to unity, the ideal AR shifts more towards 1, as such structures have more low-order polarization coefficients (with AR = 1 being the extreme that only has a p_1 with all other p_n being 0). Consequently, the same evaluation for smaller d_p (and thus also smaller H_{crit}) yields results which are further shift towards larger AR (since the higher-order polarization terms have more influence at closer H).

4.5. Ideal aspect ratio

Fig. 6 shows the critical particle diameter $d_{p,\text{crit}}$ (as evaluated according to Fig. 2a) for different AR and different starting distances from the post from $1.25 \text{ }\mu\text{m}$ to $7.5 \text{ }\mu\text{m}$. Other parameters are $d_s = 50 \text{ }\mu\text{m}$, $v_f = 4 \text{ }\mu\text{m s}^{-1}$, $E_0 = 40 \text{ kV m}^{-1}$, and $d_p = 400 \text{ nm}$. Here, a small value (hence, the possibility to trap small particles from a certain distance) corresponds to a good performance. The $d_{p,\text{crit}}$ decreases from 380 nm to 420 nm at $H = 7.5 \text{ }\mu\text{m}$ to 50 nm to 130 nm at $H = 1.25 \text{ }\mu\text{m}$. This is reasonable as the force decays with distance from the tip (independent of AR or base geometry) and is always highest at the surface of the post. Therefore, at the smallest H the particles exhibit the highest force, and it is possible to trap the smallest particles. Obviously, each curve (H) shows a minimum of $d_{p,\text{crit}}$ with AR (or an ideal AR for trapping at a certain distance H).

The ideal AR shifts towards larger values with increasing starting distance H from 0.1 at $H = 1.25 \text{ }\mu\text{m}$ to 0.4 at $H = 7.5 \text{ }\mu\text{m}$. Essentially, the explanation is the same as for Fig. 5: the smaller AR, the more higher-order polarization terms are involved in the overall polarization field generated by the post. Higher-order polarization terms generate a DEP force field that is comparably large at the surface of the post but decays fast with distance r from the post (and is thus comparably weak at distance). The contrary is true for a post

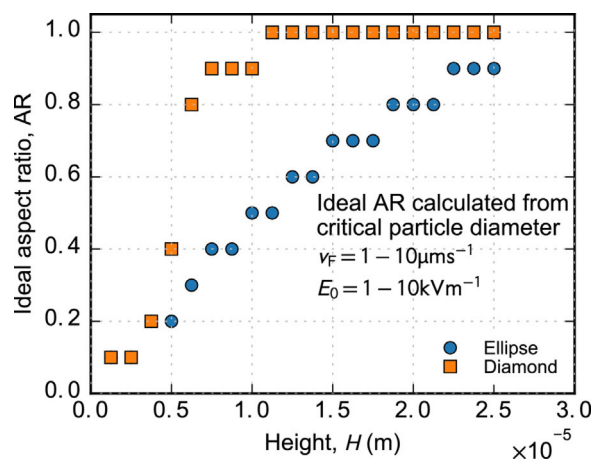


Fig. 7. Ideal aspect ratios for separation as evaluated from the minima of $d_{p,crit}(AR, H)$ curves for posts with elliptical (blue circles) and rhomboidal (orange squares) cross section at $\varepsilon_0/\varepsilon_1 = 10^4$. (For interpretation of the references to color in this figure legend, the reader is referred to the web version of the article.)

with an AR close to unity. Then, the generated force field due to the polarized post is comparably weak at the post's surface but is relatively stable with r (and thus higher at distance from the post). This two opposing effects result in an ideal AR for a specific distance H for particle trapping.

The ideal AR as a function of H is only dependent on the base geometry and $\varepsilon_0/\varepsilon_1$ but independent of other parameters, such as E_0 or v_F (Fig. 7). The figure depicts the ideal AR for posts with elliptical and rhomboidal cross section at $\varepsilon_0/\varepsilon_1 = 10^4$ as evaluated from the minima of the $d_{p,crit}(AR, H)$ curves from Fig. 6. We would like to note that we have only investigated aspect ratios with an accuracy of one digit after the decimal point. For both geometries sigmoidal dependencies of the ideal AR from H were found. But while the elliptical posts yield an almost straight line for the ideal AR, the rhomboidal posts show a much steeper rise and thus a higher or similar ideal AR at the same H . This is because the rhomboidal post shows more higher-order polarization terms compared to an elliptical post with the same AR. Hence, in order to reach a similar distribution of force over distance from the post, the rhomboidal post always has to have an AR slightly closer to one than the elliptical post. The upper limit is $AR = 1$; when $AR > 1$ the orientation of E_0 and v_F as described in Fig. 1d and e would be ineffective and $d_{p,crit}$ increases dramatically.

4.6. Sensitivity of solution towards the parameters

For a better understanding on how the key parameters influence the trapping efficiency of a specific post configuration we defined a target value H_{crit}/d_S , and investigated how it changed when the key parameters E_0 , v_F , d_S , and d_p were varied by two orders of magnitude (Fig. 8a). The target value, H_{crit}/d_S , can be understood as a trapping efficiency of the post; the larger the value the better it is possible to attract particles with less polarized material. Fig. 8a presents results for a post with elliptical cross section and the central values of $v_F = 4 \mu\text{m s}^{-1}$, $d_p = 400 \text{ nm}$, $d_S = 50 \mu\text{m}$, and $E_0 = 40 \text{ kV m}^{-1}$ for an aspect ratio of one. To make it more clear what the parameters mean, Fig. 8b shows how a channel containing a post array could look like including labeling of all parameters.

The lines for E_0 and d_p (red and orange) collapse, the H_{crit}/d_S value increases with increasing parameters. Also, the lines for d_S and v_F (green and blue) collapse, but H_{crit}/d_S decreases with increasing parameter. The collapsing lines indicate that both parameters have the same influence on H_{crit}/d_S in the investigated parameter

range, as it is also indicated by the similar first-order sensitivity indices shown in the inset of Fig. 8a. This means that the overall trapping with respect to the post size is affected by the fluid velocity in the same manner as by the overall system size, i.e., when the entire system size is doubled it has the same effect as when the fluid flow velocity past the post would be doubled.

The variation of E_0 and d_p by two orders of magnitude has a much stronger influence on H_{crit}/d_S than the variation of the d_S or v_F , which can also be inferred from larger S_1 values for d_p and E_0 (inset). The aspect ratio itself has a very small influence (S_1 value) on the overall variation of H_{crit}/d_S value compared to the other four parameters.

Generally, a large H_{crit}/d_S is desirable, because it yields large trapping range at a simultaneously small post size. A small post size is advisable because it yields a higher throughput and causes less overall electric field disturbance. At the same time it is desirable to have a small E_0 (less cost) and a large v_F (high throughput). Thus, a trade-off is required to balance all input parameters while simultaneously achieving a sufficient separation.

To summarize the findings above, the most influential parameters on the trapping efficiency are the post size d_S , the particle size d_p , the electric field strength E_0 , and the fluid flow velocity v_F . The aspect ratio AR can be used to finally adjust the structure to a specific trapping distance. The parameters are, however, not inter-changeably variable. The particle size d_p defines the problem (and thus is not variable), the aspect ratio AR and the post size d_S are geometrical design parameters, and the field strength E_0 and the fluid flow velocity v_F are operational parameters. From the presented results, some relationships appear obvious: since H_{crit}/d_S has the same sensitivity towards E_0 and d_p , it is possible to adjust towards a changing separation problem (variation in the particle size d_p to be trapped) by varying the applied voltage E_0 in a reciprocal manner.

Similarly, when the system size (d_S and the distance between two posts) changes, the fluid flow velocity v_F can or should similarly change reciprocally. It is, on the other hand, not possible to simply scale up a chromatographic separation process by changing either v_F or the system size as the target value has the same sensitivity towards both parameters. A scale up at constant particle size and separation efficiency is therefore always linked to a change in AR (small influence) or applied voltage.

Not directly evident is that a decrease in voltage and/or particle size could be absorbed by a decrease in volume flow or system size. The latter parameters (v_F , d_S) need to change much more than the former (d_p , E_0) as the process is more sensitive towards E_0 and d_p . A decrease in d_p by one order of magnitude, for instance, would cause a necessary decrease in v_F by two to three orders of magnitude (estimated, as this is not depicted in Fig. 8a).

Backing the current results with experimental data of single particle trajectories past single posts is experimentally challenging: The expected differences regarding the initial distance to the tip are in the range of the investigated particle size, even at high applied voltages. This makes a solid investigation almost impossible because the expected error in particle position is larger than the expected target value. Experimental investigations for an integral treatment focused on particle concentration rather than single particles are on the way.

4.7. Influence of a second post

Different from other studies analyzing the post arrangement and geometry influence we are investigating single posts instead of arrays; on the one hand, we thereby forfeit accuracy due to neglecting the influence that adjacent posts have on each other. On the other hand, we gain deeper knowledge and understanding of the underlying phenomena. Results with single posts are easier to analyze and comprehend because they deliver an undisturbed picture.

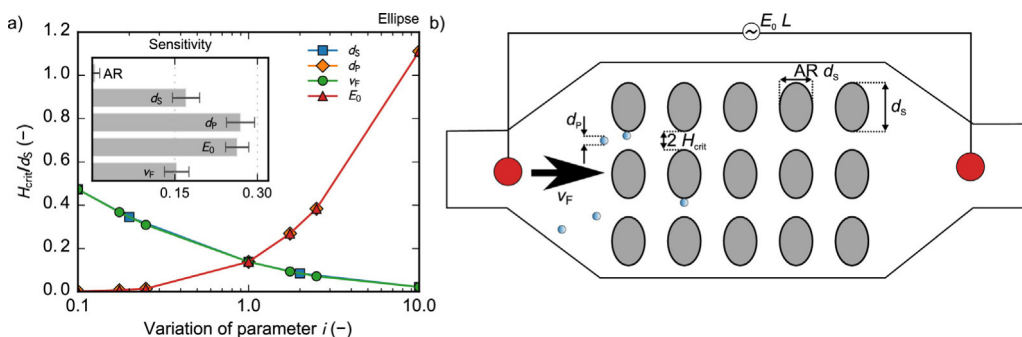


Fig. 8. (a) Ratio of critical separation height to characteristic post dimension H_{crit}/d_s for a variation of the key investigation parameters by two orders of magnitude around a base value of $v_F = 4 \mu\text{m s}^{-1}$, $d_p = 400 \text{ nm}$, $d_s = 50 \mu\text{m}$, and $E_0 = 40 \text{ kV m}^{-1}$ (aspect ratio is 1). The inset shows the first-order sensitivity index S_1 as obtained from a Sobol sensitivity analyses (performed using SALib for Python) for the five parameters that have been varied in a range between $AR = 0.1$ – 1 , $v_F = 0.4$ – $40 \mu\text{m s}^{-1}$, $d_p = 40 \text{ nm}$ – $4 \mu\text{m}$, $d_s = 5$ – $500 \mu\text{m}$, and $E_0 = 4$ – 400 kV m^{-1} . The error bars represent the confidence interval at a confidence level of 95%. (b) Example of a flow channel containing an array of posts with all the important labeling from part (a) of the figure.

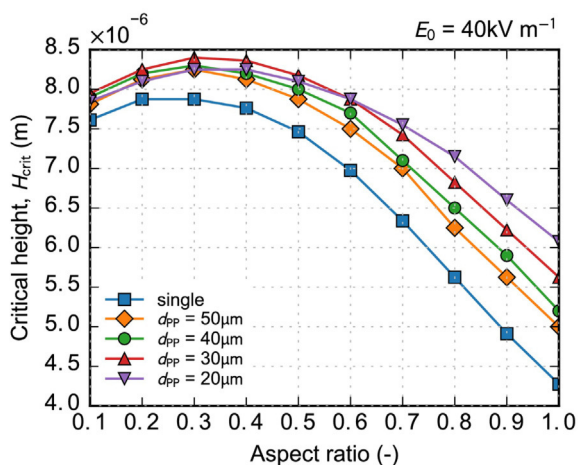


Fig. 9. Influence of a second (elliptical) post on H_{crit} at an applied excitatory field strength of $E_0 = 40 \text{ kV m}^{-1}$ (and similar parameters as in Fig. 4a) as a function of aspect ratio for different post-to-post distances from $d_{pp} = 20 \mu\text{m}$ to $50 \mu\text{m}$.

Further, they are much faster to obtain and show significantly less numerical inaccuracies.

In order to demonstrate the influence of a second, opposing post we compare the results for elliptical posts of Fig. 4a with results for two posts, which are acquired using a modeling approach that is less computational expensive but delivers results with slightly reduced accuracy. The full description is given in Section 2 of Supplementary material, briefly: a second post was placed below the first one (at the same x -coordinate) so that the distance between the top tip of the lower post and the bottom tip of the top post in y -direction is d_{pp} . The maximum distance to the tip in y -direction, H_{crit} , is again measured from the bottom tip of the top post. If a particle is still trapped at the maximum distance from either tip (it is then on the center line between the two posts, i.e., $H = d_{pp}/2$) it becomes trapped either way, and there is no H_{crit} for this specific configuration.

The introduction of a second post could, depending on E_0 and the distance d_{pp} , change the resulting H_{crit} up to 30% in either direction. The trend described in the last sections, however, is still applicable when a second post is introduced. At low voltages ($E_0 = 10 \text{ kV m}^{-1}$), a second post appears to be beneficial and H_{crit} increases with decreasing distance between the two posts, d_{pp} . At moderate voltages ($E_0 = 40 \text{ kV m}^{-1}$ and $E_0 = 70 \text{ kV m}^{-1}$) it appears that there is an ideal distance d_{pp} between the two posts for each aspect ratio.

Results for $E_0 = 40 \text{ kV m}^{-1}$ are shown in Fig. 9. Here, for instance, at $AR = 0.1$ the maximum H_{crit} is reached for $d_{pp} = 30 \mu\text{m}$ whereas for $AR = 1$, the maximum H_{crit} is reached for $d_{pp} = 20 \mu\text{m}$. At a high value of $E_0 = 100 \text{ kV m}^{-1}$, the single obstacle performs best and H_{crit}

decreases with decreasing d_{pp} , meaning, a second obstacle appears to be disadvantageous at high applied voltages.

4.8. Comparison with literature data

The group of Lapizco-Encinas published two very comprehensive studies on the influence of post characteristics on their efficiency in immobilizing particles [24,21] in channels containing arrays of insulating posts using *negative* DEP. We would like to compare our results, but would also like to highlight how our work differs from the presented references. Firstly, we are dealing with positive dielectrophoresis as opposed to negative DEP.

Also, we are not using an integral approach that relies on the trapping coefficient which also integrates electrokinetic movement apart from DEP, but focus on the movement of particles solely due to DEP. More importantly, we boiled the problem down to the most basic approach we could think of and start with only evaluating single particles next to single posts. This is an entirely different approach and helps to understand some of the underlying principles. Nevertheless, we extended the results with those containing two opposing posts and compare this with the work of Lapizco-Encinas. As presented in the next few paragraphs, albeit using quite different methods, we will find some similarities.

LaLonde et al. [24] found that for quite narrowly spaced posts (post-to-post distance is one quarter of post's characteristic dimension) the posts with diamond-shaped cross section perform better than posts with ellipsoidal cross section at an aspect ratio of 1. This is consistent with our results, at small values of H_{crit} (cf. Fig. 4) usually the rhomboidal posts perform better (larger H_{crit}).

Also, when comparing the minimum required voltage for trapping and the mean field gradient between posts, they found that the influence of the cross-sectional aspect ratio is more important for ellipsoidal posts than for posts with diamond-shaped cross section which is also consistent with our findings (again, cf. Fig. 4, the H_{crit} changes much more rapidly with AR for an ellipse than for a diamond).

Saucedo-Espinosa and Lapizco-Encinas [21] indicate that both, the electric field and the resulting field gradient, on the centerline between two posts are stronger for an elliptical post than for a rhomboidal post with a characteristic dimension of $200 \mu\text{m}$ and a post-to-post distance of $50 \mu\text{m}$. However, when comparing the minimum required voltage for trapping (Fig. 7), it is evident that diamond-shaped posts perform better in this base geometry case than ellipsoidal posts, which is also consistent with their previous results [24]. Therefore, the centerline value of the field and the field gradient does not appear to be an adequate measure for assessment of the posts performance. The variation of the gradient with y is very different for different cross-sectional post geometries.

Further, Saucedo-Espinosa and Lapizco-Encinas [21] found that their (geometrically averaged) trapping coefficient (which is a measure for the post's particle trapping effectivity) increases with decreasing aspect ratio until a maximum is reached after which the trapping coefficient decreases again with aspect ratio. This increase and maximum is more significant for ellipsoidal posts than for rhomboidal. We found the same maximum for ellipsoidal posts but cannot see it for rhomboidal except for very small distances ($d_S = 500 \mu\text{m}$ line in Fig. S1d of Supplement). We assume that the critical value shifts towards smaller aspect ratios with decreasing post-to-post distance. According to our single post studies a decreasing spacing in y -direction between posts is beneficial because it forces particles to pass the posts closer to their surface (and thus they experience a higher gradient). Studies concerning an array of posts, on the other hand, indicate that there is a specific spacing at which the performance of the array is maximum, which is supported by our investigations with two opposing posts (Fig. 9 and Section 2 of Supplementary material). These results indicate that there is an ideal distance depending on the applied voltage and the aspect ratio of the investigated post.

5. Conclusion

To conclude, we presented a method to evaluate the particle trapping potential of single posts in insulator-based (electrodeless) pDEP application using a simulative method based on the trajectories of single particles. We used this method to develop a new fundamental methodology for analyzing the influence of geometrical and operational parameters on the particle trapping efficiency of an electrodeless dielectrophoretic separation device. With the example of positive DEP we show the prediction power of our approach by giving design rules for channels containing insulating posts.

More detailed, particles were flowing past the post in a certain distance in y -direction H . A constant fluid stream of velocity v_F is dragging the particle in x -direction along the tip of the post. An excitatory (originally homogeneous) electric field causes a polarization of the post. The resultant inhomogeneous electric field depends on the geometry of the post (base geometry and aspect ratio, cf. Fig. 1b and c). This inhomogeneous field gives rise to a DEP force. Depending on, among other parameters, the size of the particle, the DEP force distribution, and the initial distance in y -direction to the tip, a particle could either pass the post without trapping or it will become trapped at the post's tip (Fig. 2).

Two main target values have been identified, the critical particle diameter $d_{p,\text{crit}}$ at constant starting distance to the tip H and the critical starting distance to the tip H_{crit} at constant d_p . The main parameters of the post geometry are the base geometry (diamond or ellipse), the aspect ratio ($AR = w/h$), and the ratio between the permittivity of the surrounding medium ε_0 and the post ε_1 , $\varepsilon_0/\varepsilon_1$.

We investigated the dependency of $d_{p,\text{crit}}$ as a function of $\varepsilon_0/\varepsilon_1$ (Fig. 3) for different base geometries and aspect ratios. Generally, the more $\varepsilon_0/\varepsilon_1$ varies from unity, the more the post becomes polarized, resulting in the possibility to trap smaller particles (smaller $d_{p,\text{crit}}$). The distribution of the force towards the post's tip as a function of distance from the tip is strongly dependent on how the resultant multipole is distributed among the order n of the polarization coefficients p_n . This distribution varies with aspect ratio (more higher-order coefficients at low AR), base geometry (more higher-order coefficients for a rhomboidal post than an elliptical) and permittivity ratio (higher-order coefficients fall faster with $\varepsilon_0/\varepsilon_1$ than low-order coefficients, cf. Fig. 5). This results in an ideal aspect ratio depending on the initial distance to the tip H (Fig. 6), which changes with base geometry (Fig. 7) or $\varepsilon_0/\varepsilon_1$ (Fig. 5).

We have further assessed how far a particle could start away from the tip of the post with size d_S for a variation of the operational parameters E_0 and v_F , cf. Fig. 4. We found that the influence of each parameter on the overall trapping efficiency can be characterized by H_{crit}/d_S using a sensitivity analysis (Fig. 8a). Here, we found that the influence of E_0 and d_p is similar. Also, the influence of v_F and d_S is similar but reciprocal. Also when varied by two orders of magnitude, E_0 and d_p appear to have the most impact on H_{crit}/d_S . In addition, the aspect ratio itself can only be used to make final adjustments on the structure for a specific target trapping distance H_{crit} .

With respect to a scale up of a separation process we could show that, at constant particle size and separation efficiency, it is not sufficient to simply adjust either v_F or the system size. In fact a simultaneous change in AR (small influence) or applied voltage is also required. We further discussed the relationships, the possibility to vary the parameters (geometrical design parameters vs. operational parameters vs. separation problem) and deduced general statements on the design of fractionation devices containing (insulating) posts.

Generally it is possible to back simulated pDEP trajectories with experimental data as we have shown elsewhere [48]. In this case, due to an extremely low ratio of critical particle-to-tip distance to the particle size, the error in the particle position is expected to be larger than the simulated H_{crit} difference.

The results presented here can be applied in the design of separation devices which rely on positive DEP and the electric field distortion at material boundaries. Typically one could think of an array of insulating posts (cf. Fig. 8b) but also constricting and diverging microchannels can be evaluated. We deliver a list of variable parameters and their influence on the overall separation. We are motivated by using these channels as particle filters and examples could be the separation of conductive particles (metal) from non-conductive particles (plastic, metal oxides, etc.) in scrap recovery or the prominent example of the separation of live and dead cells as already proposed by Pohl and Hawk [49].

Here, we consider the volume flow as separate variable and rely on pumps for fluid transport, which gives us on the one hand a broader range of parameters to investigate but is, on the other hand, mostly motivated by the wish to generate a higher throughput which is more easily achievable when DEP movement and movement through the channel are decoupled. Particle trajectory simulations through such channels together with experimental validation in microchannels are on the way.

We believe that these single post–single particle investigations on the one hand help understanding and rationalizing the underlying phenomena of post polarization and DEP particle movement. On the other hand we deliver a tool for designing electrodeless dielectrophoresis devices for positive DEP attraction of particles in arrays of posts (or similar designs) in microfluidic systems.

Acknowledgements

GRP would like to thank Lars Kiewidt (University of Bremen, UFT) for his assistance in solving differential equations and performing sensitivity analysis. GRP is also member of the Research Training Group (GRK 1860) "Micro-, meso-, and macroporous non-metallic materials" of the German Research Foundation (DFG).

Appendix A. Supplementary data

Supplementary data associated with this article can be found, in the online version, at <http://dx.doi.org/10.1016/j.chroma.2016.12.074>.

References

- [1] H.A. Pohl, *Dielectrophoresis*, Cambridge University Press, London/New York/Melbourne, 1978.
- [2] R. Pethig, Review article – dielectrophoresis: status of the theory, technology, and applications, *Biomicrofluidics* 4 (2010) 1–35.
- [3] R. Pethig, Dielectrophoresis: an assessment of its potential to aid the research and practice of drug discovery and delivery, *Adv. Drug Deliv. Rev.* 65 (2013) 1589–1599.
- [4] Z. Gagnon, S. Senapati, J. Gordon, H.-C. Chang, Dielectrophoretic detection and quantification of hybridized DNA molecules on nano-genetic particles, *Electrophoresis* 29 (2008) 4808–4812.
- [5] R. Hölzel, N. Calander, Z. Chiragwandi, M. Willander, F. Bier, Trapping single molecules by dielectrophoresis, *Phys. Rev. Lett.* 95 (2005) 128102.
- [6] L.A. Flanagan, J. Lu, L. Wang, S.A. Marchenko, N.L. Jeon, A.P. Lee, E.S. Monuki, Unique dielectric properties distinguish stem cells and their differentiated progeny, *Stem Cells* 26 (2008) 656–665.
- [7] H. Morgan, N. Green, *Dielectrophoresis*, in: *Encyclopedia of Microfluidics and Nanofluidics*, Springer New York, New York, NY, 2015, pp. 563–572.
- [8] R. Krupke, F. Henrich, H.B. Weber, M.M. Kappes, H.V. Löhneysen, Simultaneous deposition of metallic bundles of single-walled carbon nanotubes using ac-dielectrophoresis, *Nano Lett.* 3 (2003) 1019–1023.
- [9] B. Bharti, O.D. Velev, Assembly of reconfigurable colloidal structures by multidirectional field-induced interactions, *Langmuir* (2015).
- [10] S. Molla, S. Bhattacharjee, Dielectrophoretic levitation in the presence of shear flow: implications for colloidal fouling of filtration membranes, *Langmuir* 23 (2007) 10618–10627.
- [11] F. Du, A. Hawari, M. Baune, J. Thöming, Dielectrophoretically intensified cross-flow membrane filtration, *J. Membr. Sci.* 336 (2009) 71–78.
- [12] F. Du, P. Ciaciuch, S. Bohlen, Y. Wang, M. Baune, J. Thöming, Intensification of cross-flow membrane filtration using dielectrophoresis with a novel electrode configuration, *J. Membr. Sci.* 448 (2013) 256–261.
- [13] A.H. Hawari, F. Du, M. Baune, J. Thöming, A fouling suppression system in submerged membrane bioreactors using dielectrophoretic forces, *J. Environ. Sci.* 29 (2015) 139–145.
- [14] H. Morgan, N.G. Green, *AC Electrokinetics: colloids and nanoparticles*, 1st ed., Research Studies Press, Baldock, 2002.
- [15] N.G. Green, T.B. Jones, Numerical determination of the effective moments of non-spherical particles, *J. Phys. D: Appl. Phys.* 40 (2007) 78–85.
- [16] G.R. Pesch, L. Kiewidt, F. Du, M. Baune, J. Thöming, Electrodeless dielectrophoresis: impact of geometry and material on obstacle polarization, *Electrophoresis* 37 (2016) 291–301.
- [17] K.-T. Liao, M. Tsegaye, V. Chaurey, C.-F. Chou, N.S. Swami, Nano-constriction device for rapid protein preconcentration in physiological media through a balance of electrokinetic forces, *Electrophoresis* 33 (2012) 1958–1966.
- [18] B.G. Hawkins, B.J. Kirby, Electrothermal flow effects in insulating (electrodeless) dielectrophoresis systems, *Electrophoresis* 31 (2010) 3622–3633.
- [19] I. Barbulovic-Nad, X. Xuan, J.S.H. Lee, D. Li, DC-dielectrophoretic separation of microparticles using an oil droplet obstacle, *Lab Chip* 6 (2006) 274–279.
- [20] P. Zellner, T. Shake, Y. Hosseini, D. Nakidde, M.V. Riquelme, A. Sahari, A. Pruden, B. Behkam, M. Agah, 3D Insulator-based dielectrophoresis using DC-biased, AC electric fields for selective bacterial trapping, *Electrophoresis* 36 (2015) 277–283.
- [21] M. Saucedo-Espinosa, B. Lapizco-Encinas, Design of insulator-based dielectrophoretic devices: effect of insulator posts characteristics, *J. Chromatogr. A* 1422 (2015) 325–333.
- [22] M.A. Saucedo-Espinosa, A. LaLonde, A. Gencoglu, M.F. Romero-Creel, J.R. Dolas, B.H. Lapizco-Encinas, Dielectrophoretic manipulation of particle mixtures employing asymmetric insulating posts, *Electrophoresis* 37 (2016) 282–290.
- [23] R.C. Gallo-Villanueva, V.H. Pérez-González, R.V. Davalos, B.H. Lapizco-Encinas, Separation of mixtures of particles in a multipart microdevice employing insulator-based dielectrophoresis, *Electrophoresis* 32 (2011) 2456–2465.
- [24] A. LaLonde, A. Gencoglu, M.F. Romero-Creel, K.S. Koppula, B.H. Lapizco-Encinas, Effect of insulating posts geometry on particle manipulation in insulator based dielectrophoretic devices, *J. Chromatogr. A* 1344 (2014) 99–108.
- [25] B.H. Lapizco-Encinas, B.A. Simmons, E.B. Cummings, Y. Fintschenko, Dielectrophoretic concentration and separation of live and dead bacteria in an array of insulators, *Anal. Chem.* 76 (2004) 1571–1579.
- [26] J.-S. Kwon, J.-S. Maeng, M.-S. Chun, S. Song, Improvement of microchannel geometry subject to electrokinesis and dielectrophoresis using numerical simulations, *Microfluid. Nanofluid.* 5 (2007) 23–31.
- [27] C.-P. Jen, T.-W. Chen, Selective trapping of live and dead mammalian cells using insulator-based dielectrophoresis within open-top microstructures, *Biomed. Microdev.* 11 (2009) 597–607.
- [28] C.-P. Jen, C.-T. Huang, H.-Y. Shih, Hydrodynamic separation of cells utilizing insulator-based dielectrophoresis, *Microsyst. Technol.* 16 (2009) 1097–1104.
- [29] S. Kazemlou, N. Nazemifard, Electric field gradients during electrophoretic fractionation in microfabricated post arrays, *Microfluid. Nanofluid.* 17 (2014) 993–1002.
- [30] I. Ermolina, H. Morgan, The electrokinetic properties of latex particles: comparison of electrophoresis and dielectrophoresis, *J. Colloid Interface Sci.* 285 (2005) 419–428.
- [31] C. Prinz, J.O. Teegenfeldt, R.H. Austin, E.C. Cox, J.C. Sturm, Bacterial chromosome extraction and isolation, *Lab Chip* 2 (2002) 207–212.
- [32] C.-F. Chou, J.O. Teegenfeldt, O. Bakajin, S.S. Chan, E.C. Cox, N. Darnton, T. Duke, R.H. Austin, Electrodeless dielectrophoresis of single- and double-stranded DNA, *Biophys. J.* 83 (2002) 2170–2179.
- [33] J. Regtmeier, T.T. Duong, R. Eichhorn, D. Anselmetti, A. Ros, Dielectrophoretic manipulation of DNA: separation and polarizability, *Anal. Chem.* 79 (2007) 3925–3932.
- [34] J. Regtmeier, R. Eichhorn, L. Bogunovic, A. Ros, D. Anselmetti, Dielectrophoretic trapping and polarizability of DNA: the role of spatial conformation, *Anal. Chem.* 82 (2010) 7141–7149.
- [35] A. Nakano, T.C. Chao, F. Camacho-Alanis, A. Ros, Immunoglobulin G and bovine serum albumin streaming dielectrophoresis in a microfluidic device, *Electrophoresis* 32 (2011) 2314–2322.
- [36] M.A. Mata-Gómez, R.C. Gallo-Villanueva, J. González-Valdez, S.O. Martínez-Chapa, M. Rito-Palomares, Dielectrophoretic behavior of PEGylated RNase A inside a microchannel with diamond-shaped insulating posts, *Electrophoresis* 37 (2016) 519–528.
- [37] J. Regtmeier, R. Eichhorn, M. Viefhues, L. Bogunovic, D. Anselmetti, Electrodeless dielectrophoresis for bioanalysis: theory, devices and applications, *Electrophoresis* 32 (2011) 2253–2273.
- [38] S.K. Srivastava, A. Gencoglu, A.R. Minerick, DC insulator dielectrophoretic applications in microdevice technology: a review, *Anal. Bioanal. Chem.* 399 (2011) 301–321.
- [39] G.R. Pesch, F. Du, U. Schwientek, C. Gehrmeier, A. Maurer, J. Thöming, M. Baune, Recovery of submicron particles using high-throughput dielectrophoretically switchable filtration, *Sep. Purif. Technol.* 132 (2014) 728–735.
- [40] C. Iliescu, G. Xu, F.C. Loe, P.L. Ong, F.E.H. Tay, A 3-D dielectrophoretic filter chip, *Electrophoresis* 28 (2007) 1107–1114.
- [41] R. Wakeman, G. Butt, An investigation of high gradient dielectrophoretic filtration, *Chem. Eng. Res. Des.* 81 (2003) 924–935.
- [42] J. Suehiro, G. Zhou, M. Imamura, M. Hara, Dielectrophoretic filter for separation and recovery of biological cells in water, *IEEE Trans. Ind. Appl.* 39 (2003) 1514–1521.
- [43] Y. Wang, F. Du, M. Baune, J. Thöming, Dielectrophoresis in aqueous suspension: impact of electrode configuration, *Microfluid. Nanofluid.* (2014).
- [44] H. Nili, N.G. Green, Higher-order dielectrophoresis of nonspherical particles, *Phys. Rev. E* 89 (2014) 063302.
- [45] J.D. Jackson, *Klassische Elektrodynamik*, 5th ed., Walter de Gruyter, Berlin, Boston, 2013.
- [46] J.L. Baylon-Cardiel, B.H. Lapizco-Encinas, C. Reyes-Betanzo, A.V. Chávez-Santoscoy, S.O. Martínez-Chapa, Prediction of trapping zones in an insulator-based dielectrophoretic device, *Lab Chip* 9 (2009) 2896–2901.
- [47] A. Ramos, P.G. A-Sánchez, H. Morgan, AC Electrokinetics of conducting microparticles: a review, *Curr. Opin. Colloid Interface Sci.* 24 (2016) 79–90.
- [48] Y. Wang, F. Du, G.R. Pesch, J. Köser, M. Baune, J. Thöming, Microparticle trajectories in a high-throughput channel for contact-free fractionation by dielectrophoresis, *Chem. Eng. Sci.* 153 (2016) 34–44.
- [49] H.A. Pohl, I. Hawk, Separation of living and dead cells by dielectrophoresis, *Science* 152 (1966) 647–649.